ADVANCED MATERIALS TECHNOLOGIES
www.advmattechnol.de

A Triboelectric Nanogenerator-Based Smart Insole for Multifunctional Gait Monitoring

*Zhiming Lin, Zhiyi Wu, Binbin Zhang, Yi-Cheng Wang, Hengyu Guo, Guanlin Liu, Chaoyu Chen, Yuliang Chen, Jin Yang, and Zhong Lin Wang**

Accurately monitoring human gait is critical for health evaluation and/or early diagnosis, especially for elder and injured people's healthcare. The presence of gait abnormalities could be important predictors of the risk of developing diseases. Herein, a triboelectric nanogenerator (TENG)-based smart insole for real-time gait monitoring is reported. Due to the novel air-pressure-driven structural design, the elastic TENG-based sensors exhibit compelling features including simple fabrication, fast response time, high durability, and excellent mechanical robustness. The TENG-based sensors can be easily integrated into the conventional insole so that it can convert the mechanical triggering/impact into electrical output. By analyzing such electrical signals, the smart insole could accurately monitor and distinguish various gait patterns in real time, including jump, step, walk, and run. The smart insole could also be used to monitor the abnormality of gait for rehabilitation assessment. In addition, the smart insole can play another important role in healthcare applications, for example, serving as a fall-down alert system for elder people or patients. This work not only paves a new way for real-time and long-term gait monitoring, but also presents a new perspective for the practical applications of remote clinical biomotion analysis.

1. Introduction

With the rapid development of modern society, increasingly rapid pace of life today might affect human health.[1,2] Along with the population aging problem facing the world, gait monitoring has attracted increasing attention, especially for health monitoring and early diagnosis.[3,4] For example, the presence of gait abnormalities could be an important predictor for the risk of developing dementia.[5] Effective gait monitoring can also be used in various health-related occasions, such as fall risk estimation, assessment of recovery, and the ambulatory monitoring for Parkinson's disease.[6,7] In addition, researchers have shown that gait monitoring devices can be used in sport training that can improve the performance of athletes, including golf, running, and baseball training.[8–10] Due to the demand for these versatile applications, intensive efforts have been devoted on gait monitoring with various strategies and working mechanisms.[11–15] The camera-based method is one of the most effective methods to observe gait motions.[13] However, it has spatial and temporal restrictions that limit the analysis to be at a specific time and/or in a confined location. Force-plate instrumented treadmills may also provide such information, but they are expensive and limited to laboratory settings. Accelerometers/gyroscopes offer a lightweight and portable approach for gait monitoring, nevertheless, the accelerometer-based method cannot provide quantitative and accurate results for gait analysis.[14] Thus, developing novel technologies for gait monitoring with the characteristics of wearable, easy to use, low cost, and accurate recognition remains challenging.

Triboelectric nanogenerator (TENG) is a kind of device that can convert mechanical energy into electrical output, taking advantage of contact electrification and electrostatic induction.[16] It has been demonstrated as a promising alternative for both mechanical energy harvesting[17–23] and self-powered active sensing[24–30] due to its various advantages, such as high power density, high efficiency, low cost, and lightweight. A liquid metal droplet based triboelectric nanogenerator has been reported as a self-powered sensor for human gait monitoring and analyzing.[31] However, that sensor could not recognize various gait patterns and only can detect them by frequency. In addition, the liquid metal mercury droplet used in the devices may pose potential threats to human body and not suitable for mass production due to the potential environmental pollution.

Dr. Z. Lin, Dr. Z. Wu, Dr. B. Zhang, Dr. Y.-C. Wang, Dr. H. Guo, Dr. G. Liu, Dr. C. Chen, Dr. Y. Chen, Prof. Z. L. Wang
School of Materials Science and Engineering
Georgia Institute of Technology
Atlanta, GA 30332-0245, USA
E-mail: zhong.wang@mse.gatech.edu
Dr. Z. Lin, Prof. J. Yang
Key Laboratory of Optoelectronic Technology and Systems
(Ministry of Education)
Department of Optoelectronic Engineering
Chongqing University
Chongqing 400044, P. R. China
Prof. Z. L. Wang
Beijing Institute of Nanoenergy and Nanosystems
Chinese Academy of Sciences
Beijing 100083, P. R. China
The ORCID identification number(s) for the author(s) of this article can be found under https://doi.org/10.1002/admt.201800360.

DOI: 10.1002/admt.201800360

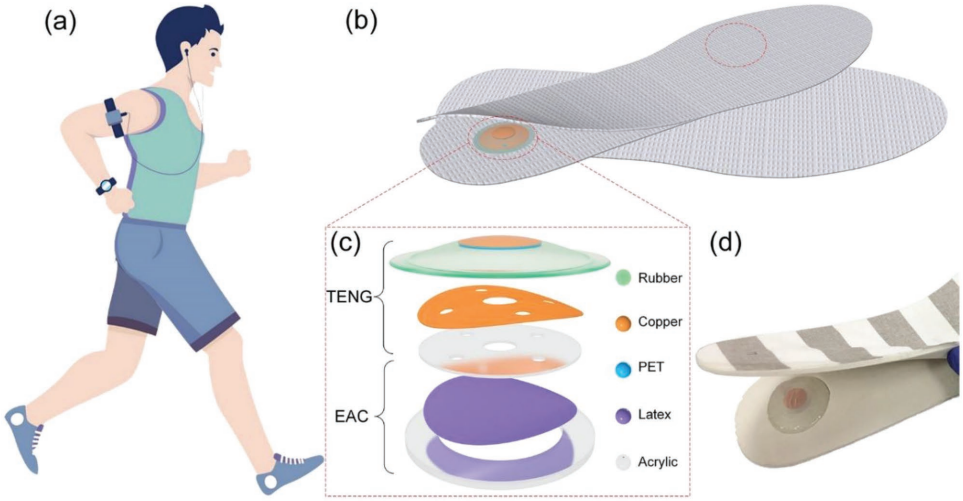

Figure 1. Overview of the smart insole for gait monitoring. a) The smart insoles assembled into the shoes to serve as a self-powered gait monitoring system. b) The TENG-based sensors integrated in the front and rear of the insoles. c) The layer-by-layer structural design of the TENG-based sensor. d) A photograph of the as-fabricated smart insole.

To address this issue, in this work, an ease-of-use and wearable smart insole based on triboelectric nanogenerators was developed for real-time multifunctional gait monitoring. The smart insole consists of two novel designed triboelectric sensors located in the front and rear of the insole. Each triboelectric sensor is composed of two parts: a TENG (convex) part on top of an elastic air chamber (EAC) part, which is made of a designed elastic latex film. The TENG part consists of a rubber layer and a copper layer, with another copper layer embedded in the rubber layer to reduce undesired signal induced by environmental factors. In general, TENGs rely on the contact-separation event happened between two triboelectric layers (rubber layer and copper layer, in this case) to convert the mechanical triggering into electrical output. Different from the abovementioned TENG reported previously that utilizing the restoring force of the selected material to trigger the contact and separation events between the two triboelectric layers, our designed triboelectric sensor takes advantage of the air pressure within the sealed device, to achieve such events. When an external force is applied, two triboelectric layers are in contact with each other and the air in the (convex) TENG part will be squeezed to the bottom elastic air chamber part. As the mechanical force is released, the bottom elastic latex film could drive the air back to the top convex to achieve separation between two triboelectric layers (original state). Through this structure design, the smart insole exhibits a fast response time of less than 56 ms compared with previous reported device, which is beneficial for real-time gait monitoring. Additionally, the electrical output shows a negligible decrease over 1000 cycles, evidently presenting excellent stability and mechanical durability. Based on the time difference of the forefoot and heel of the foot contact with ground, various gait patterns such as step, walk, and run can be recognized and monitored, which is different from the reported TENGs monitoring the gait by output amplitude and frequency. Through the changes of the time difference between two feet, the treatment of the disease advancing state or health condition will be accurately monitored. More importantly, upon an unexpected fall-down event occurs, the wearable smart insole could detect it immediately, rendering it feasible as intelligent healthcare products. With the features of wearable, ease of use, fast response as well as accurate recognition, the smart insole presents a more convenient alternative for human gait monitoring and evaluation, which could be widely adopted in motion tracking and medical healthcare systems.

2. Results and Discussion

Figure 1a,b shows the illustration of the smart insoles for human gait monitoring. Two TENG-based sensors are integrated in the front (underneath the ball of foot) and rear (underneath rear foot) of the insole, respectively (Figure 1b). The sensor consists of a multilayered structure, including two main parts: a TENG part and an EAC part, as sketched in Figure 1c. The TENG part is composed of two major layers. A convex cambered rubber film with 20 mm diameter acts as the top layer, with a layer of copper integrated in it as a shielding layer to prevent interference from the environment. Another copper film was attached on top of the supporting acrylic layer to serve as the bottom layer of the TENG. When the external pressure was applied onto the TENG-based sensor, the rubber film was then in contact with the bottom copper film resulting in contact electrification (more working mechanisms of TENG-based sensor will be discussed in the next paragraph).

The elastic air chamber part is a layer of highly stretchable latex film serving as an elastic chamber to hold the air from the TENG temporary. Since the sensor was packed and encapsulated completely by elastomer, upon applying an external force, the air in the TENG part is squeezed, therefore, the air flows to the designed elastic air chamber part leading to the expansion of the latex film. When the external force is released, the air can flow back to the convex TENG part, leading to the separation of the two triboelectric layers. This design can also prevent water permeation from environment or sweat. The overall design not

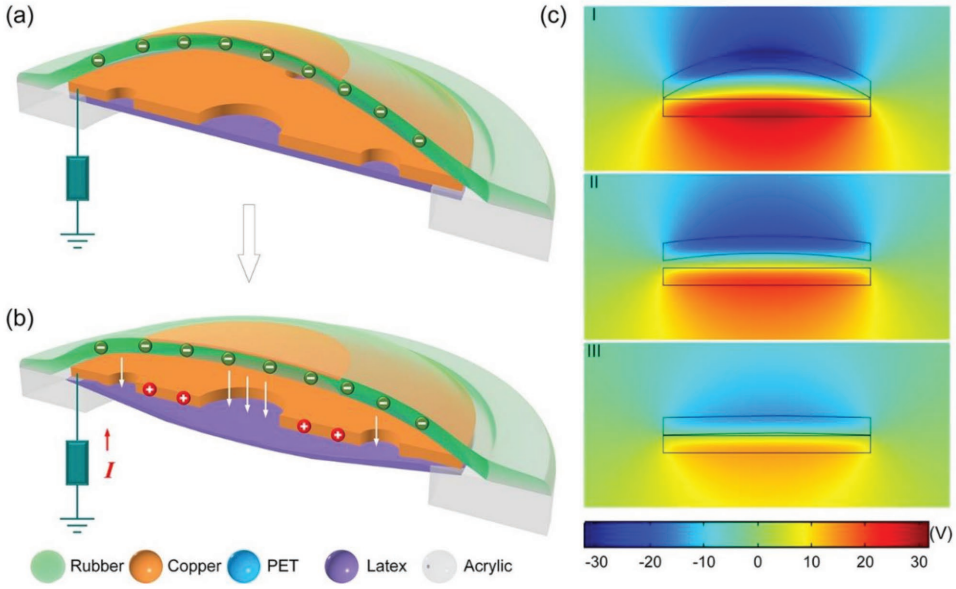

Figure 2. Electrical signal generation process of the TENG-based sensor under applied force. a) 3D illustration of the working mechanisms of the TENG-based sensor. b) Potential distribution for the distance between two triboelectric layers (or air gap) changes from 2 to 0.1 mm.

only possesses structural simplicity that could be compatible with conventional manufacturing processes, but also provides excellent robustness, making the sensor more reliable and durable in practical scenarios. A photograph of an as-fabricated smart insole based on triboelectric sensors is exhibited in Figure 1d. The detailed fabrication processes are discussed in the Experimental Section.

The working mechanisms of the TENG-based sensor rely on contact and separation between two triboelectric layers (i.e., rubber layer and copper layer). Taking advantage of the design, which can couple triboelectrification and electrostatic induction giving rise to alternating flow of the electrons. The electricity-generating process is depicted in **Figure 2**. Since the copper is more triboelectrically positive than rubber, electrons are transferred from copper electrode on the surface of rubber film. When the two triboelectric layers contact with each other, the negative charges will be accumulated on the rubber side. These triboelectric charges are nonmobile and could sustain on the surfaces for a long period of time, as shown in Figure 2a.

When the TENG-based sensor is pressed by an external force, the two triboelectric layers come closer (the distance between the two layers will become smaller). As the charged rubber layer comes closer toward the copper layer, the electrons transfer from the copper film surface to the ground due to the change of electrical field, as demonstrated in Figure 2b. Then electrons will flow through the load and finally reach an equilibrium. The detailed electrical signal generation processes could be found in Figure S1 (Supporting Information). We also conducted simulations of the potential distribution using COMSOL. The results for the distance between two triboelectric layers (or air gap) from 2 to 0.1 mm are demonstrated in Figure 2c correspondingly, which agrees well with the above theory. Additionally, the acquired voltage and current signals of the TENG based sensor in the press and release states are displayed in Figure S2 (Supporting Information).

To characterize the electrical output performances of the TENG-based sensor, a computer-controlled linear motor was employed. In addition, a force gauge was used to measure the applied force. First, the open-circuit voltage outputs with different applied forces were investigated to understand the response of this TENG-based sensor to normal forces. As can be seen in **Figure 3**a, the amplitude of the output voltage rises linearly with increasing forces at a constant frequency of 3 Hz. Larger force can lead to better contacted between the elastomeric rubber layer and the copper film, thus a higher electrical output can be obtained. For example, when the lowest applied force (5 N) was used, the voltage output was 7 V; however, when the highest applied force (40 N) was exploited, the voltage output raised to 35 V (Figure 3a). These results also imply that it can detect very low external force (5 N). Figure 3b demonstrates the relationship between short-circuit-current outputs of the sensor and applied force, which has a similar trend to the open-circuit voltage in Figure 3a. Subsequently, we investigated the effects of the operating frequencies on the output performance of the TENG-based sensor. As can be seen from Figure 3c, the open-circuit voltage is almost the same, about 35 V, at different operating frequencies. However, the short-circuit current increases from 0.05 to 0.25 μA as the operation frequency increases. In other words, the increase in frequency is favorable for the magnitude of the short-circuit current. The reason is that the transferred charges are constant under various operating frequencies, whereas the contact time between two layers of TENGs changes at different operating frequencies. Therefore, the short-circuit current output of the TENGs would change. For example, a higher operating frequency can lead to a higher flow rate of charges, resulting in a higher current output.

It is well-known that pressing objects (foot, hand, etc.) can naturally carry some charges on their surfaces, which could be generated by the contact-electrification process happening with

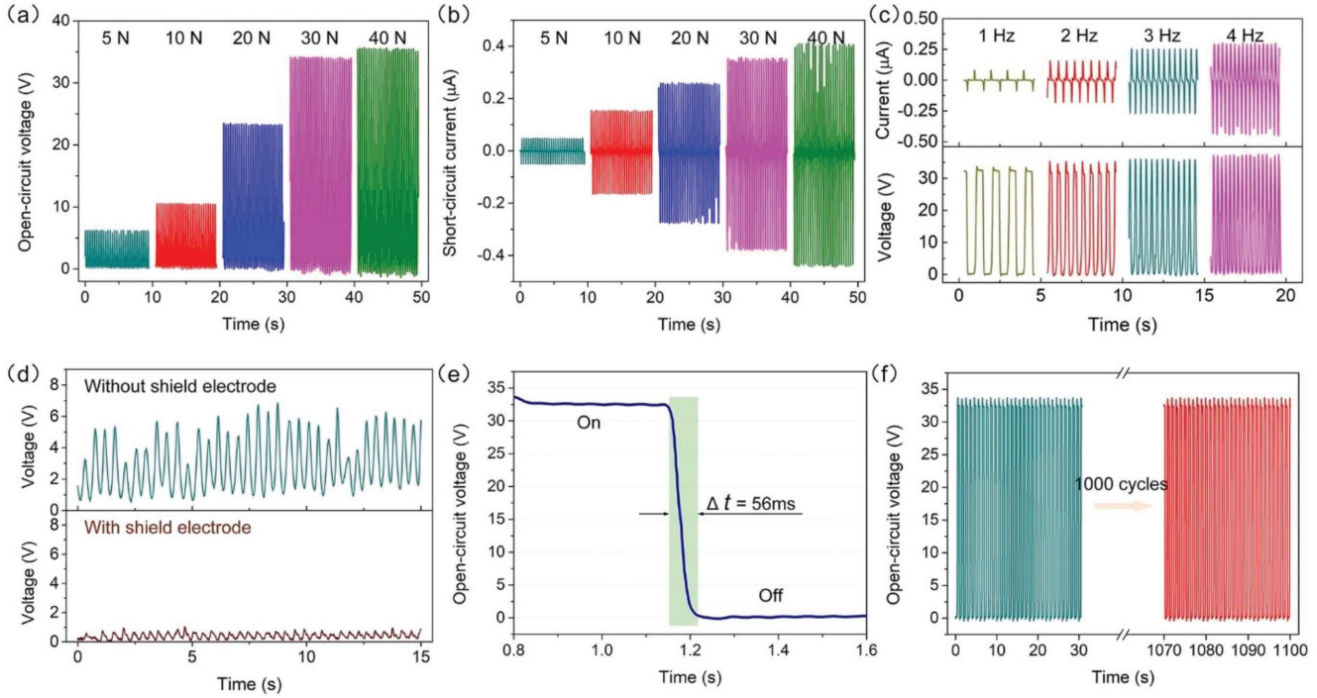

Figure 3. Electrical and mechanical characterization of the TENG-based sensor. a) Open-circuit voltage and b) short-circuit current at different applied forces. c) Electrical output (current and voltage) of the sensor at various pressing frequencies. d) Comparison of the output signals with and without shield electrode. e) Time response of the voltage in one cycle (external force applied and released: on and off). f) The mechanical durability characterization of one unit of the TENG-based sensor with ≈1000 continuous working cycles.

other objects or even with air.[28,32] The surface charges on these objects can also induce additional output signals, due to the electrostatic induction. Thus, to minimize the undesired signals from the environment, a copper thin film was integrated into the rubber film and connected to the ground to serve as the shielding electrode (Figure 1c). The electrical outputs of the sensor with and without the shielding electrode were tested by hand-pressing/releasing. Figure 3d shows that the unwanted voltage components induced from pressing object (e.g., fingers) were greatly reduced with the shield electrode. That is, the output signals from the device with the shielding electrode are the ones that generated majorly from the interactions of different triboelectric layers within the sensor, not from any other undesired environmental factors. Hence, the shield electrode in our designed smart insole plays a key role of promoting signal accuracy by minimize the unwanted environmental factors.

To further investigate the performance of our TENG-based device, the response time of the sensor to external forces was also examined. Figure 3e shows the voltage output from applying an external loading to releasing it, exhibiting a response time of less than 56 ms under the force of 30 N. and the time response of the TENG-based sensor under different applied forces are shown in Figure S3 (Supporting Information). The rapid response ensures the sensor can detect the signal in time when external force presents. Additionally, the stability of the TENG-based sensor was characterized by applying/releasing a force of 30 N for 1000 cycles. As can be seen from Figure 3f, the almost constant open-circuit voltage amplitude indicates the stability and durability of the sensor. Moreover, as shown in Figure S4 (Supporting Information), the output voltages remained nearly constant after 5000 cycles' test under greater forces, showing a significant device robustness. To summarize the performances of the TENG-based sensor, it demonstrates a great force detection sensitivity, fast response time, and significant device robustness, which justify the practicability of the sensor for gait monitoring.

To demonstrate the smart insole can serve as a sensing device for practical scenarios, a real-time gait monitoring system is developed. The system consists of a pair of smart insoles based on triboelectric sensors, a multichannel data acquisition system, and the designed data monitoring and analyzing software. The signals generated from different sensors in the smart insole can be detected and recorded simultaneously, which are transmitted by the wire connected to multichannel data acquisition system. As shown in **Figure 4**a, when the forefoot steps on the floor, a negative peak is generated from front part of the insole (i.e., from the front TENG-based sensor in the insole). Similarly, a positive peak can be detected when the forefoot step off the floor. Interestingly, the time difference (t) between the negative peak and positive peak can be another critical factor for subtle gait monitoring. With the addition of anther TENG-based sensor on the rear of the sole, the time difference between front and rear sensors is also another critical parameter for the recognition and analysis of gait patterns.

Based on analyzing the abovementioned traits of the negative/positive peaks using our designed software, various gait patterns: stepping, walking, and running, can be recognized and distinguished, as demonstrated in Figure 4b,c. Figure 4b shows the gait signals of stepping. It can be seen that the right heel and forefoot lift sequentially when stepping, corresponding

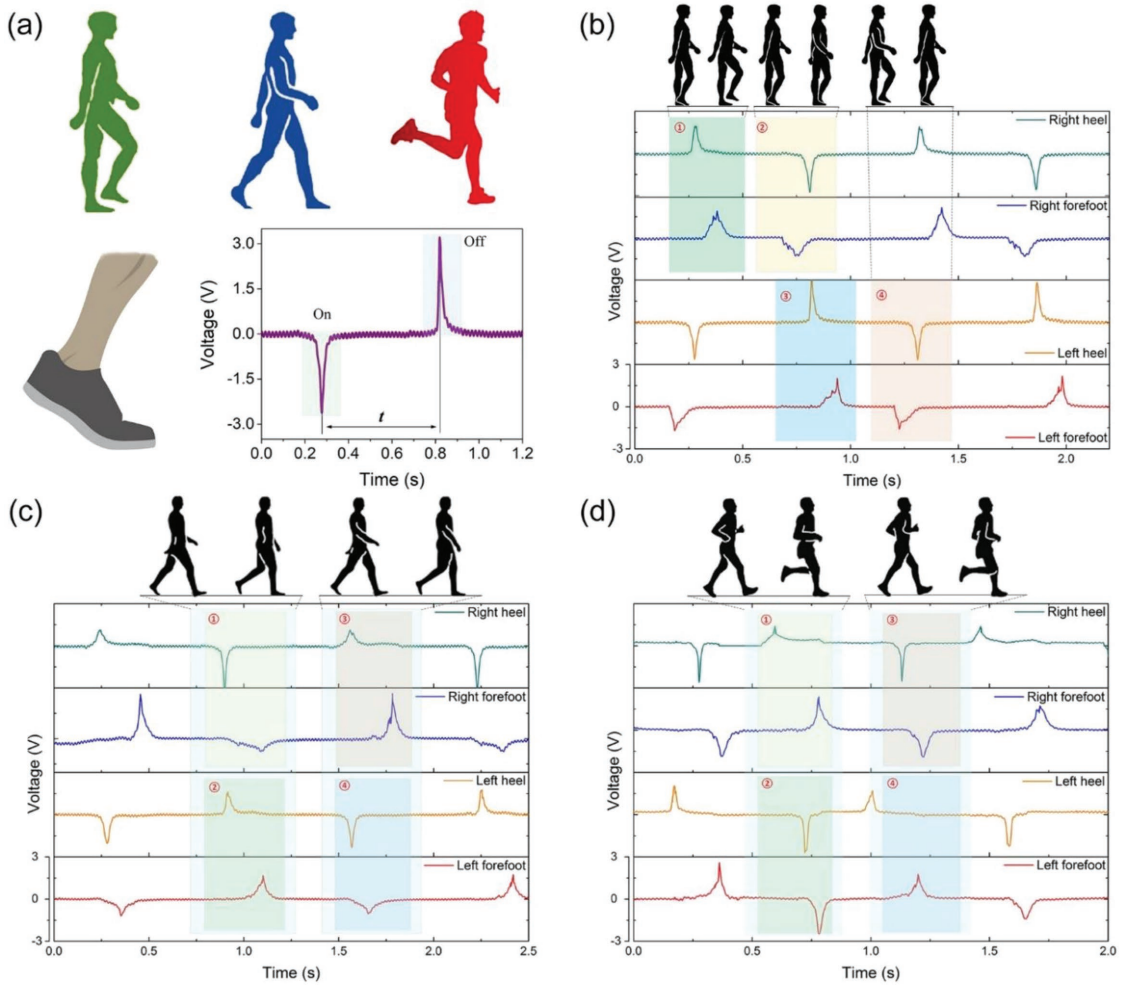

Figure 4. The gait monitoring signals of the smart insoles. a) Typical detected signals when the foot step is on and off. Sensing signals for different gait patterns: b) stepping, c) walking, and d) running.

to the positive peaks in region ①. Then the right foot naturally lands on the ground, as depicted in region ②. The right forefoot lands on the ground first, followed by the right heel landing. In the meantime, the left foot lifts from the ground with the similar sequence to the right foot, as demonstrated in region ③. Then the left foot also lands on the ground with the same sequence of forefoot first, followed by heel (region ④). This is the full cycle of signal generation progress of stepping.

The gait pattern of walk can also be characterized by the monitoring system. As the right heel lands on the ground, the left heel and forefoot lifts from the ground sequentially. Meanwhile, the right forefoot also lands on the ground, as systemically demonstrated in Figure 4c. The sensing signals of run are the same as those of walk, however, the frequency of the run is significantly higher than that of walk (i.e., the time different between the positive and negative peaks is much shorter), as shown in Figure 4d. We also examined the jump signals to demonstrate the capability of distinguishing various gait using our monitoring system. As can be seen from Figure S5 and Video S1 (Supporting Information), the signals of the right and left heels are generated simultaneously, and then the signals of the right and left forefoot also appear at the same time. These results not only indicate that the gait patterns can be easily distinguished by our system, but also suggest that smart insole can be further adopted for motion tracking, activity recognition, sports training, and various other applications.

In addition to the basic gait recognition, herein, we demonstrate an example on how the smart insole can be used on sport training, taking advantage of its fast response time, light weight, and wearable properties. Specifically, the smart insole was used to monitor the gait of triple jump, as shown in **Figure 5**a. It could be found that the gait of both feet was recorded at each stage (approach, hop, skip, and jump). The corresponding peaks and response time (t_h, t_s, and t_j), could be further analyzed to evaluate every athlete's motion for his/her improvement in the training, without using any high-speed video camera system or other expensive equipment. For example, does the athlete run on the right speed that can maintain his/her forward and height momentum; or does the athlete take off/land on the right foot/timing/position?

Additionally, providing detailed gait information for the patients with gait disorders or injury is getting increasing important for clinical gait analysis and/or rehabilitation assessment. It has been reported that the gait pattern of ankle

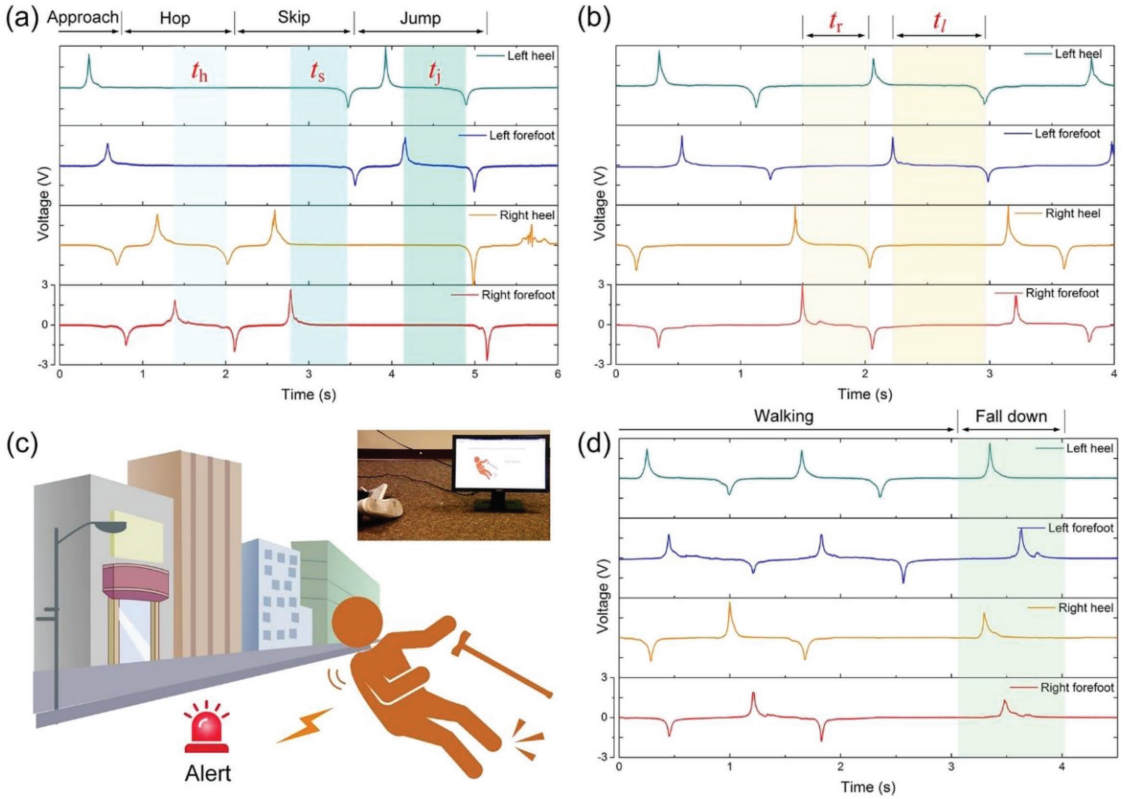

Figure 5. Demonstrations of the smart insoles for a) triple jump training, b) gait rehabilitation treatment, and c,d) warning of fall down.

or keen injured person may be different from that of the healthy person.[33] Thus, we mimicked the gait pattern of a left ankle injured (sprain) person (i.e., by walking with a slower motion and not putting too much pressure one foot) and used a pair of the smart insoles to monitor the gait of an injured person. The recorded real-time gait behavior signals are displayed chromatically in Figure 5b. It clearly elucidates the time spent of every step for the right foot t_r and left foot t_l, indicating that the time difference. By comparing the time spent between right foot t_r and left foot t_l, the injury condition or rehabilitation of the patient could be monitored and analyzed.

On top of the clinical treatment application, our devise has a potential in medical health care monitoring application. For example, it can be used as an emergency fall detection alert system, as the system diagram elucidated in Figure 5c. When an elder people or patient falls down, the smart insole can detect the event in real time and send an alarm immediately. Figure 5d shows an example of real-time recorded gait signals for a fall-down event detected by the smart insole. First, a typical walk gait signal was detected, then four positive peaks from the TENG-based sensors were emerged at the same time, indicating both feet off the ground, demonstrated in the inset of Figure 5c and Video S2 (Supporting Information). Based on the distinct signals from the sensor, the smart insole could recognize the fall-down event in real time. This demonstration shows a great potential of our smart insole in medical applications, especially in real-time remote healthcare monitoring system, and emergency medical alert system for elder people and patients. With further optimization of the gait monitoring, it is anticipated that the monitoring system would be further integration such as wireless transmission with greatly improved wearing comfort in the field of healthcare monitoring.

3. Conclusions

In summary, we demonstrated a wearable, easy-to-use smart insole based on TENG for real-time gait monitoring. Compared to existing gait monitoring devices, our novel approach addresses some major limitations of the current technologies, such as high cost, difficult-to-use or difficult-to-install, and/or special limitations. With the desirable features, such as wearable, rapid response, decent durability, and easy-to-fabricate, the TENG-based sensor enabled smart insole not only can achieve realize real-time gait monitoring, but also may be suitable for mass production. More importantly, the designed smart insole is capable of distinguishing various gait patterns, such as jump, step, run, and walk. The collected data from the smart insole may also be applied to the analysis of patients' gait for rehabilitation assessment. In addition, this smart insole can serve as alert system for fall-down events detection, which could be important for patients and elder people. This study demonstrates a novel design in wearable devices for gait monitoring, which can further contribute to the design of activity recognition, remote healthcare monitoring, and other health evaluation devices.

4. Experimental Section

Fabrication of the Triboelectric Nanogenerator-Based Sensor: An acrylic sheet was first processed by laser cutting and sculpting (TR-6040) to form a spherical groove with 20 mm in diameter. Then, silicone rubber solution (Ecoflex 00-50) (1:1, volume ratio) was drop-casted onto the spherical groove to form a convex cambered rubber film. A layer of copper thin film serving as a shielding layer was placed on the rubber film. Subsequently, the cambered rubber film coated with copper was dip-coated with another silicone rubber layer as the triboelectric layer. An acrylic plate was cut into a disk shape (20 mm in diameter) with five holes for air flow. Another thin copper film was attached on the surface of the tailored acrylic plate. Then, the acrylic plate was tightly adhered underneath the cambered rubber film made previously. Finally, a layer of highly stretchable latex film was prepared and which was sandwiched by the tailored acrylic plate and acrylic circular ring to form an elastic air chamber.

Electrical Characterization and Mechanical Measurement: A dual-range force sensor (Vernier Software & Technology, LLC) was employed to measure the force applied onto the TENG-based sensor. The open-circuit voltage was measured by a Keithley system electrometer (Keithley 6514), and the short-circuit current was measured by using an SR570 low noise current amplifier (Stanford Research System), respectively. Informed consent was obtained from the participant, who volunteered to perform these studies. All testing reported conformed to the ethical requirements of Georgia Institute of Technology.

Supporting Information

Supporting Information is available from the Wiley Online Library or from the author.

Acknowledgements

Z.L., Z.W., and B.Z. contributed equally to this work. The authors are grateful for the supports received from the Hightower Chair Foundation of the Georgia Institute of Technology, the "Thousands Talents" program for pioneer researcher and his innovation team in China, and the National Natural Science Foundation of China (Grant Nos. 51432005, 5151101243, and 51561145021). The authors also acknowledge the China Scholarship Council for supporting research at Georgia Institute of Technology.

Conflict of Interest

The authors declare no conflict of interest.

Keywords

shielding effect, smart shoes, triboelectric nanogenerator (TENG), triboelectric sensors, wearable electronics

Received: August 16, 2018
Revised: September 12, 2018
Published online:

[1] Z. Ma, *Science* **2011**, *333*, 830.
[2] C. Dagdeviren, Y. Su, P. Joe, R. Yona, Y. Liu, Y.-S. Kim, Y. Huang, A. R. Damadoran, J. Xia, L. W. Martin, *Nat. Commun.* **2014**, *5*, 4496.
[3] L. Atallah, A. Wiik, G. G. Jones, B. Lo, J. P. Cobb, A. Amis, G.-Z. Yang, *Gait Posture* **2012**, *35*, 674.
[4] J. Bae, M. Tomizuka, *Mechatronics* **2013**, *23*, 646.
[5] J. Verghese, R. B. Lipton, C. B. Hall, G. Kuslansky, M. J. Katz, H. Buschke, *N. Engl. J. Med.* **2002**, *347*, 1761.
[6] J. Bae, K. Kong, N. Byl, M. Tomizuka, *J. Biomech. Eng.* **2011**, *133*, 041005.
[7] J. L. Riskowski, *Gait Posture* **2010**, *32*, 242.
[8] L. Wang, W. Hu, T. Tan, *Pattern Recognit.* **2003**, *36*, 585.
[9] K. Y. Chen, K. F. Janz, W. Zhu, R. J. Brychta, *Med. Sci. Sports Exercise* **2012**, *44*, S13.
[10] W. Tao, T. Liu, R. Zheng, H. Feng, *Sensors* **2012**, *12*, 2255.
[11] J. Rueterbories, E. G. Spaich, B. Larsen, O. K. Andersen, *Med. Eng. Phys.* **2010**, *32*, 545.
[12] A. Muro-De-La-Herran, B. Garcia-Zapirain, A. Mendez-Zorrilla, *Sensors* **2014**, *14*, 3362.
[13] E. Stone, M. Skubic, *J. Ambient Intell. Smart Environ.* **2011**, *3*, 349.
[14] B. R. Greene, D. McGrath, R. O'Neill, K. J. O'Donovan, A. Burns, B. Caulfield, *Med. Biol. Eng. Comput.* **2010**, *48*, 1251.
[15] C.-C. Yang, Y.-L. Hsu, *Sensors* **2010**, *10*, 7772.
[16] F.-R. Fan, Z.-Q. Tian, Z. L. Wang, *Nano Energy* **2012**, *1*, 328.
[17] G. Zhu, J. Chen, T. Zhang, Q. Jing, Z. L. Wang, *Nat. Commun.* **2014**, *5*, 3426.
[18] J. Yang, J. Chen, Y. Yang, H. Zhang, W. Yang, P. Bai, Y. Su, Z. L. Wang, *Adv. Energy Mater.* **2014**, *4*, 1301322.
[19] J. Yang, J. Chen, Y. Liu, W. Yang, Y. Su, Z. L. Wang, *ACS Nano* **2014**, *8*, 2649.
[20] Z. Lin, J. Chen, X. Li, Z. Zhou, K. Meng, W. Wei, J. Yang, Z. L. Wang, *ACS Nano* **2017**, *11*, 8830.
[21] S. Niu, X. Wang, F. Yi, Y. S. Zhou, Z. L. Wang, *Nat. Commun.* **2015**, *6*, 8975.
[22] J. Chen, Y. Huang, N. Zhang, H. Zou, R. Liu, C. Tao, X. Fan, Z. L. Wang, *Nat. Energy* **2016**, *1*, 16138.
[23] C. Xu, Y. Zi, A. C. Wang, H. Zou, Y. Dai, X. He, P. Wang, Y. C. Wang, P. Feng, D. Li, *Adv. Mater.* **2018**, *30*, 1706790.
[24] J. Yang, J. Chen, Y. Su, Q. Jing, Z. Li, F. Yi, X. Wen, Z. Wang, Z. L. Wang, *Adv. Mater.* **2015**, *27*, 1316.
[25] Z. Lin, J. Yang, X. Li, Y. Wu, W. Wei, J. Liu, J. Chen, J. Yang, *Adv. Funct. Mater.* **2018**, *28*, 1704112.
[26] Z. Wu, W. Ding, Y. Dai, K. Dong, C. Wu, L. Zhang, Z. Lin, J. Cheng, Z. L. Wang, *ACS Nano* **2018**, *12*, 5726.
[27] W. Ding, C. Wu, Y. Zi, H. Zou, J. Wang, J. Cheng, A. C. Wang, Z. L. Wang, *Nano Energy* **2018**, *47*, 566.
[28] C. Wu, W. Ding, R. Liu, J. Wang, A. C. Wang, J. Wang, S. Li, Y. Zi, Z. L. Wang, *Mater. Today* **2018**, *21*, 216.
[29] P. Wang, R. Liu, W. Ding, P. Zhang, L. Pan, G. Dai, H. Zou, K. Dong, C. Xu, Z. L. Wang, *Adv. Funct. Mater.* **2018**, *28*, 1705808.
[30] J. Chen, Z. L. Wang, *Joule* **2017**, *1*, 480.
[31] B. Zhang, L. Zhang, W. Deng, L. Jin, F. Chun, H. Pan, B. Gu, H. Zhang, Z. Lv, W. Yang, *ACS Nano* **2017**, *11*, 7440.
[32] S. Li, W. Peng, J. Wang, L. Lin, Y. Zi, G. Zhang, Z. L. Wang, *ACS Nano* **2016**, *10*, 7973.
[33] J. L. Astephen, K. J. Deluzio, G. E. Caldwell, M. J. Dunbar, *J. Orthop. Res.* **2008**, *26*, 332.